High-throughput cell focusing and separation via acoustofluidic tweezers

Mengxi Wu[a,b], **Kejie Chen**[b], **Shujie Yang**[a], **Zeyu Wang**[a], **Po-Hsun Huang**[a], **John Mai**[c], **Zeng-Yao Li**, and **Tony Jun Huang**[*,a]

[a]Department of Mechanical Engineering and Material Science, Duke University, Durham, NC 27707 USA

[b]Department of Engineering Science and Mechanics, Pennsylvania State University, University Park, PA 16802 USA

[c]Alfred Mann Institute for Biomedical Engineering, University of Southern California, Los Angeles, CA 90007, USA

Abstract

Separation of particles and cells is an important function in many biological and biomedical protocols. Although a variety of microfluidic-based techniques have been developed so far, there is clearly still a demand for a precise, fast, and biocompatible method for separation of microparticles and cells. By combining acoustics and hydrodynamics, we have developed a method which we integrated into three-dimensional acoustofluidic tweezers (3D-AFT) to rapidly and efficiently separate microparticles and cells into multiple high-purity fractions. Compared with other acoustophoresis methods, this 3D-AFT method significantly increases the throughput by an order of magnitude, is label-free and gently handles the sorted cells. We demonstrate not only the separation of 10, 12, and 15 micron particles at a throughput up to 500 μl/min using this 3D-AFT method, but also the separation of erythrocytes, leukocytes, and cancer cells. This 3D-AFT method is able to meet various separation demands thus offering a viable alternative with potential for clinical applications.

Introduction

Separation of micron-scale particles and cells is a critical step for a variety of protocols used in many biological and biomedical studies. Because its length scales can be matched with microparticles and cells, the development of microfluidic technology is strongly motivated by the needs to separate biomolecules and cells, ever since its infancy.[1] This has led to the blossoming of numerous microfluidic separation techniques over the past several decades.[2,3] Until now, a variety of microfluidic platforms have been developed, including surface affinity-based separation,[4] hydrodynamic filtration,[5,6,7] pinch flow fractionation,[8] cross-flow filtration,[9] deterministic lateral displacement,[10] inertial microfluidics,[11,12] micro centrifugation,[13] optical tweezers,[14] electrophoresis,[15,16] dielectrophoresis,[17] magnetophoresis,[18] and acoustophoresis.[19] These separation methods rely on various

---

[*] tony.huang@duke.edu.

mechanisms that can be categorized into two groups: utilizing either the dynamic fluidic force or by applying external forces. Each mechanism has its advantages and disadvantages. Among all the aforementioned techniques, acoustophoresis emerges as unique due to its label-free, contact-free, and gentle operation. These characteristics make it a promising tool for the practical separation of bioparticles and cells.

In general, acoustophoresis primarily utilizes an acoustic radiation force to manipulate particles in a fluid. The balance between the acoustic radiation force and the fluidic drag force controls the motion of particles and cells to relocate at certain positions based on their sizes and densities. One method to introduce an acoustic radiation force into a fluid is to generate standing acoustic waves in a half-wavelength acoustic resonator that is precisely fabricated using silicon or other hard materials and the excitation source is a ceramic-based piezo transducer.[20–22] Another approach is by using interdigital transducers (IDTs) rather than bulk transducers to generate surface acoustic waves (SAWs) on piezoelectric substrates. [23–25] By positioning the IDTs with respect to the channel position on the substrate, the generated acoustic pressure nodes can be aligned in the desired positions within the microfluidic channel. However, in both cases the channel dimensions need to be scaled correctly with the acoustic wavelength. More importantly, the maximum separation distance for the particles is restricted to less than half the wavelength, which increases the probability that particles are directed to the wrong outlets. Recently, a novel tilted-angle design has been reported whereby the distance that the particles are deflected via the acoustic radiation force can be increased beyond this wavelength restriction.[26] D. Collins et. al combined acoustic force with dielectrophoresis force to generate more deflection of particles thus improved the separation efficiency.[27]

Even though advances have been made, several limitations remain. Firstly, acoustophoresis relies on the focusing of particles prior to separation, which is usually achieved by using a sheath flow. The sample-to-sheath flow ratio is typically about 1:10, which significantly limits the processing throughput. [20,21,25] Although the total flow rate can be over 100 μl/min, after deducting the sheath flow component from total flow rate, the sample flow rate is ~10 μl/min which is often not sufficient for rapid separation. Antfolk et. al[22] reported sheath-less focusing and separation where the inlet flow rate was set to be 100 μl/min. However, two transducers with different working frequencies were used which makes their electronics setup more complicated than our control system. Secondly, the variation in particle position in the vertical direction results in velocity differences due to the flow profile in a microfluidic channel. Specifically, particles near a solid surface of the channel flow slower than those in the center. This natural velocity gradient affects separation performance since the time for particles to travel through the active region, and the resulting lateral deflection distance, is not a constant. Thirdly, the deflection distances of particles are still limited even with the recent tilted-angle technique. Further increasing the deflection distance will improve purity and furthermore resulting in the ability to separate multiple components simultaneously.

In this work, we present a novel method, 3D-AFT, which is capable of sorting and separating micro particles and cells into multiple fractions with a high throughput, with a sample flow rate up to 500 μl/min. Leveraging the advantages of hydrodynamics and

acoustics, this method sequentially achieved both lateral and vertical focusing and then finally sorting (Figure 1). Specifically, particles that are randomly distributed within a rectangular microchannel are first directed into an asymmetric serpentine channel. In this module (i.e., hydrodynamic-based lateral focusing module), the inertial component of the flow becomes significant, and thus the lift force dominates the migration of particles, aligning particles into a single stream in the lateral direction.[28] However, particles are often focused to two equilibrium positions in the vertical direction.[29] A. Chung et. al proposed a way to achieve single-focal plane using an inertial focusing mechanism, however, this method requires a complicated channel geometry with different step heights repeated 30 times.[30] In this work, particles that focused in two vertical positions enter an acoustic resonator formed by hybrid microchannel. In this module (i.e., acoustic-based vertical focusing module), the primary acoustic radiation force pushes the particles towards a pressure node thus aligning them in a single line in the vertical direction. After particles are focused in three dimensions by hydrodynamic and acoustic mechanisms, they are directed to the third module (i.e., acoustic-based separation module). In this module, a balance of the fluidic drag force and acoustic radiation force in the lateral direction controls the motion of particles. Therefore, particles are separated based on their size and density. This method can separate micro particles and cells in a continuous manner without exposing the biological specimens to excessive fluidic shear forces. By using this method, we have increased the sample processing throughput to 500 μl/min, which is the highest throughput reported using a single, enclosed microfluidic device. We achieved the separation of 10, 12, and 15 μm particles simultaneously. In addition, we demonstrated the separation of leukocytes from erythrocytes and the separation of cancer cells from leukocytes. These results demonstrate the clinical potential of 3D-AFT as a novel device for separating a variety of microparticles and cells.

Materials and methods

Device fabrication

The fabrication process for this 3D-AFT device was similar to our previous work.[24,26] A photo of the device is shown as Figure S1. Briefly, a pair of metal IDTs were patterned on a LiNbO$_3$ substrate via photolithography, e-beam evaporation and lift-off processes. A microchannel mold was fabricated using SU8 photoresist (MicroChem, USA) and patterned via photolithography. An 800 μm × 5 mm slide glass slide, laser-cut from a micro cover glass (VWR, USA), was placed on the mold structure at a designated position. Then PDMS base and curing agent (Dow Corning, USA) were mixed at a ratio at 10:1 and poured onto the mold. After baking at 65°C for an hour, the PDMS channel with the embedded glass slide was peeled off from the mold, and then bonded to a LiNbO$_3$ substrate using a plasma treatment. Following bonding, the device was baked at 110 °C overnight.

Blood and cells

Fresh human blood was purchased from Zen-Bio, Inc. USA and used immediately upon its arrival. To distinguish erythrocytes and leukocytes, blood was diluted 300 times in PBS, and then DAPI (4',6-diamidino-2-phenylindole; Sigma-Aldrich Inc.) was added to stain the cell nucleus.

To obtain purified leukocytes, red blood cells were lysed using RBC lysis buffer (BioLegend, USA). Whole blood was mixed with the lysis buffer in a volume ratio of 1:10. The mixture was incubated at room temperature for 10 min and then centrifuged at 800 g. The supernatant was removed and the cell pellet was re-suspended using PBS. Then the leukocytes were fixed by 4% paraformaldehyde solution for 30 min. Afterwards, the fixed leukocytes were re-suspended in a PBS solution and stored at 4°C.

HeLa and HEK-293T cells were were purchased from the American Type Culture Collection and cultured with DMEM/Ham's F-12 50/50 Mix (Life Technologies, USA) supplemented with 10% (vol/vol) FBS and 1% penicillin–streptomycin solution. These cancer cells were labeled with Calcein-AM (Invitrogen, USA) for rapid identification as a control. We incubated the cells with 1 μM Calcein-AM in $1\times$ PBS solution at room temperature for 15 min. After separation SYTOX™ Orange cell stain reagent (ThermoFisher, USA) was added at 1:1000 volume ratio to identify dead cells.

Experimental setup

The 3D-AFT separation device can either be placed on the stage of an inverted microscope (Eclipse Ti, Nikon, Japan) or an upright microscope (BX51WI, Olympus, Japan) equipped with a Peltier cooling system (TEC1–12730, Hebei I.T., China). The temperature of the Peltier cooling system was controlled by using a variable DC power supply (TP1505D, Tekpower, USA). The cooling system kept temperature of fluid constant to preserve the viability of cells. A CCD camera (Nikon DS-Qi2, Nikon, Japan) was employed to record the separation process. For detailed analysis, a fast camera (Fastcam Mini AX, Photron, USA) was used in place of the normal CCD camera to acquire high-speed images. The fluid flow rate was controlled by syringe pumps (neMESYS, cetoni GmbH, Germany). Before each experiment, the microfluidic channel was flushed with ethanol to remove air bubbles in the channel, followed by a PBS wash to remove residual ethanol. In order to prevent adsorption of particles onto the channel surface, the channel was filled with 0.5 % bovine serum albumin (Sigma-Aldrich, USA) solution for 5 min to block the wetted surfaces. The SAWs were generated by applying a radio frequency signal to the IDTs on the $LiNbO_3$ substrate. The signal was supplied by a function generator (E4422B, Agilent, USA) coupled to an amplifier (Amplifier Research, USA), and was monitored by an oscilloscope (DPO4104, Tektronix, USA).

Image processing

The videos and images acquired by the CCD camera and the fast camera were processed and analyzed using ImageJ (NIH, USA). To present a time-elapsed track of the particles, a sequence of video frames were captured and then stacked, or digitally superimposed, into one image.

Results

Three-dimensional focusing of particles

In the hydrodynamic-based lateral focusing module, by using the asymmetric serpentine channel, particles that were randomly distributed would be focused into a stream in the

lateral direction; however, there were two equilibrium positions for the particles in the vertical direction. In order to form a single-file particle stream in the vertical direction, the serpentine channel exits into a section of glass/PDMS hybrid channel that forms a vertical acoustic resonator (i.e., acoustic-based vertical focusing module). The operating principle for this hybrid channel based resonator is shown in Figure 2(a). Firstly, SAWs are generated on the piezoelectric substrate by the IDTs. The vib rating solid surface in turn excites longitudinal acoustic waves in the fluid medium. The leaky waves travel in the fluid and reach the ceiling of the microfluidic channel, upon which, the leaky waves are then reflected back into the fluid by the glass/water interface since there is a significant acoustic impedance mismatch between glass and water. The reflected wave interferes with the incident wave thus generating a set of standing waves. Figure 2(b) is the numerical simulation result showing the time averaged acoustic pressure within the rectangular resonator section of the microfluidic channel. The simulation is based on a previously report numerical model, [31] with appropriate modifications to the boundary condition settings with respect to the current material properties. Note that an acoustic pressure node is formed. In this situation, the acoustic radiation force, F_r, can be expressed by Equation (1):

$$\mathbf{F_r} = -\left(\frac{\pi \mathbf{p}^2 \mathbf{V} \beta_f}{2\lambda}\right) \phi \sin(2\mathbf{kL}) \quad (1)$$

where p, V, β_f, λ, Φ, k, and L are the pressure amplitude, particle volume, acoustic wavelength, acoustic contrast factor, wave vector, and distance from the pressure node, respectively. The direction of the acoustic radiation force is determined by the acoustic contrast factor (ϕ).

$$\phi = \frac{5\rho_p - 2\rho_f}{2\rho_p + \rho_f} - \frac{\beta_p}{\beta_f} \quad (2)$$

where ρ_p, ρ_f, β_p and β_f are the density of the particles and fluid, compressibility of the particles and fluid, respectively. For most particles and cells, the acoustic contrast factor is positive, which means particles are pushed towards acoustic pressure nodes by the radiation force. As a result, by using acoustic forces, particle streams that are initially located in two different positions can be aligned to the pressure node, thus forming a single aligned and focused stream.

We tested the three-dimensional focusing performance by using 15 μm and 10 μm polystyrene beads. The flow rate was set at 200 μl/min. When the SAWs were not activated, particles flowed in a stream, where some of the particles were dark but others were clear when observing under a microscope. This indicates that particles were located at two different planes along the vertical direction. Once the acoustic waves were activated, all the

particles appeared clear, indicating that all the particles were now aligned on the same plane. We characterized the vertical positions of particles when acoustic wave is off and on, as shown in Figure S2. Without acoustic waves, particles located at two planes at 10~20 μm or 40~50 μm above the bottom of the channel. When the acoustic wave was activated, all particles were focused at the position of ~40 μm height. These results demonstrate that by combining a hydrodynamic focusing module followed by an acoustic-based vertical focusing module, the particles can be focused three-dimensionally.

Modulation of particle motion via 3D-AFT

After passing through the two focusing modules, the particles are now in a single file stream prior to entering the separation module. The three-dimensional focusing of particles enables the separation module to distinguish between different types of particles more precisely and efficiently. In the separation module, the motions of particles are modulated, as shown in Figure 3(a). The fractionation of particles relies on the combined effect of acoustics and hydrodynamics. Prior to the separation region, the particles and fluid flow in a straight channel, which suggests that the particle velocity (v_p) is equal to the bulk fluid velocity (v_f). However, the change in channel geometry changes these conditions. In the trapezoidal channel, v_f alters its direction and decreases as the channel width expands due to mass flow continuity. While v_p maintains its initial orientation since the particle follows its inertial motion for a short distance. In this case, the particle experiences a Stokes drag force from the fluid, which can be expressed as Equation (3):

$$F_d = -3 \pi \eta dv \quad (3)$$

where η is the viscosity of the fluid, d is the diameter of the particle, and v represents the relative velocity of particle with respect to the fluid. The fluid drag force tends to keep particle motion coincident with the fluid stream line, while the acoustic radiation force (F_r) pulls the particle towards an acoustic pressure node. The balance of these two forces determines the path of a particle. If the acoustic radiation force is too small, the particle trajectory will be dominated by the drag force and thus follow the fluid streamlines, whereas if the radiation force is greater than the drag force, particles will be pulled towards the pressure nodes. Note that the acoustic radiation force is not a constant and decreases as a particle moves towards a pressure node. As a result, the particle will be stable at a given position where the acoustic radiation force is equal to the drag force. Besides these two situations, the particle motion is in between these conditions.

We then experimentally validated this 3D-AFT mechanism, as shown in Figure 3(b). The flow rate was set at 200 μl/min and 15 μm polystyrene beads were used. By changing the input power of acoustic signal, the acoustic pressure intensity was adjusted, and therefore the acoustic radiation force could be tuned. The trajectories indicate that within the 3D-AFT separation device, the particle motion could be modulated. Particles were deflected from their original pathlines by the acoustic force. When the acoustic power was OFF ($F_r = 0$) or negligible ($F_r \ll F_d$), the particles followed the fluid stream line. As the acoustic power increased, the particle trajectory started to deviate from the streamline. As the acoustic

power kept increasing, the particle trajectory was diverted closer to the line of acoustic pressure nodes. At a local maximum power input, then the largest deflection angle was reached. Since the deflection angle could be controlled as a function of the input power, particles could be directed to different channel outlets.

Characterization of deflection distance and separation efficacy

In order to determine the optimal operating parameters, we characterized the correlations between the lateral deflection distance, the acoustic power, and the sample flow rate. At the exit of the channel, outside of the acoustic active region, the lateral position of the particle was no longer actively being altered. The particle motions at the outlet region were recorded under different conditions. Figure 4(a) shows the time-elapsed stacked images of the particle positions under various conditions. The input power was changed from 21 dBm to 27 dBm, and the flow rate ranged from 100 μl/min to 500 μl/min. The diameter of the particles was 15 μm. Using the situation where there was no SAW input as a reference zero, we calculated the deflection distance for the other operating conditions. Figure 4(b) shows a plot of the deflection distance as a function of the input power and flow rate for 15 μm, 12 μm, and 10 μm polystyrene beads. Generally, as the input power increased, the deflection distance became larger. Note that for 15 μm beads, the deflection distance first increased slowly between 100 and 140 μm; however, once passing a threshold power, the distance jumped to ~280 μm. This is because the acoustic radiation force exceeded the fluid drag force at that exact point, thus the deflection angle of particle trajectory was maximized. However, for 12 μm and 10 μm beads, the transition threshold was not reached over the range of experimental conditions that were investigated. The reason is due to the decreasing effective acoustic radiation force with respect to the drag force. As shown by Equation (1) and (3), when the diameter of a particle decreases, the acoustic radiation force decreases more quickly than the drag force. So for smaller particles, the acoustic radiation force has less impact than for larger particles. Therefore, the deflection distances for 12 μm and 10 μm beads were very small. Under some conditions, 12 μm particles could only be deflected by ~120 μm, while the deflection distance of 10 μm beads did not exceed 80 μm. The results indicated that particles with different sizes performed differently in a 3D-AFT device. However, different sized particles could still be distinguished and separated into different fractions in a label-free manner.

We then performed the separation of mixtures that contained 10 μm / 12 μm particles and 12 μm / 15 μm particles. The purity of output sample was characterized by dividing the number of target particles by number of total particles. The results are shown in Figure 4(c) and (d). It is noted that the separation performed well even when the throughput reaches as high as 500 μl/min. We achieved >80% purity for both 10 μm and 12 μm particles. When separating 12 μm and 15 μm particles, the purity level dropped due to ~75% when the flow rate was >300 μl/min.

Separation of erythrocytes, leukocytes, and cancer cells

It has been demonstrated that different particles migrate to different lateral positions in the 3D-AFT chip, and therefore, size-based separation of particles can be achieved. We next will

demonstrate that biological cells can be similarly sorted by separating blood cell components and cancer cells using the 3D-AFT chip.

Firstly, we separated erythrocytes and leukocytes. Fresh human blood was first diluted 300 times in a PBS solution, and then the cell nucleus staining dye DAPI was added into the mixture to identify nucleated cells. After this staining, leukocytes were now fluorescently labeled while erythrocytes were not because they lack a nucleus. The mixture was directed into the 3D-AFT separation chip. The flow rate was set as 100 μl/min. The bright field and fluorescent micrographs at the outlet region are shown as Figure 5(a). Most of the cells were erythrocytes, which were not fluorescent. A small portion of cells that were fluorescent, indicating the presence of leukocytes, were deflected down to the bottom outlet. Therefore, these results demonstrate the successful separation of leukocytes and erythrocytes.

Next, the separation of cancer cells from a population of leukocytes was performed. A cancer cell line (HeLa) was spiked into a sample of leukocytes. Before spiking, the HeLa cells were stained with Calcium-AM, which expresses a green fluorescence. The flow rate for the cell mixture was set at 200 μl/min. The separation results were also examined under a microscope. Figure 5(b) shows the stack images taken from a time-elapsed video frame capture at the outlet region for the bright field and the fluorescent field. Noted that the larger HeLa cells migrated a large distance due to the stronger acoustic radiation force and finally entered the bottom outlet, while leukocytes were directed to the top outlet because of relatively small deflected distance. With its unique characteristics in terms of being label-free and having a high throughput while preserving the cell integrity, this technique can potentially be a viable alternative approach for circulating tumor cells (CTC) isolation for cancer diagnosis, phenotyping, therapeutic drug screening and other clinical applications.

We also collected cells and examined short-term and long-term cell viability (Figure S3). Cells maintain their viability and are able to proliferate after flowing through the device and treated with acoustic waves.

Separation of multiple particles via 3D-AFT

In addition to the ability to separate particles/cells of interest into two fractions, this 3D-AFT separation technique is also capable of separating multiple types of particles simultaneously.

A mixture containing 10 μm, 12 μm and 15 μm polystyrene beads were successfully sorted. The 10 μm and 15 μm beads in this mixture were fluorescently-modified with Cy3 and FITC, respectively, for easy visualization of the device's effectiveness. Without acoustics, these three types of particles were mixed in one stream (Figure S4). With the acoustic wave activated, the mixture was separated into three fractions, as show in Figure 6. The bright-field images show that the particle mixture is sorted into three streams at the three corresponding outlets (Figure 6a). From the fluorescent images, it is clear that the three streams are entirely 10 μm, 12 μm, and 15 μm beads, respectively. The smallest fraction, 10 μm beads, entered the outlet (1), while the largest fraction, 15 μm beads, were deflected furthest and directed to the outlet (3). Because 12 μm beads have a bead size that is between 10 and 15 μm, they were moderately deflected and thus most were directed to the outlet (2). We also characterized the proportions of each size of the beads collected from three outlets.

Figure 6(b) shows that the majority of components collected in outlet 1, 2, and 3 are 10, 12, and 15 μm beads, respectively. Specifically, the purity for each size of beads is 87.6%, 88.4%, and 83.8%, respectively. These results demonstrate that the 3D-AFT based separation device is able to precisely separate particles/cells into multiple fractions in a single step.

Discussions

A broad range of compelling applications from biological to biomedical studies continuously motivates the development of advanced separation technology. These applications demand features such as precision, speed, and biocompatibility. These requirements are achieved by 3D-AFT separation, which is the combination of acoustics and hydrodynamics, as demonstrated in this article. The use of the hydrodynamic inertial force and an acoustic vertical resonator successfully focused particles to a single line both horizontally and vertically. Then within a trapezoid-shaped microchannel, the separation of different fractions was achieved due to the combined effect of the hydrodynamic drag force and the acoustic radiation force. The 3D-AFT method has been proved capable of separating microparticles and a variety of cells.

The 3D-AFT technique has also shown its ability to separate multiple fractions rapidly (500 μl/min) within a single step. When multiple particle sizes were present, by adjusting the input power to the acoustic transducers, different fractions were aligned to multiple exit channels. The largest particles migrated to the stable acoustic pressure node position. The smallest particles followed the fluid stream line and the other particles were modulated towards intermediate positions. With careful device design and acoustic parameter control, particles were directed to different outlets for collection. This feature is extremely useful in applications such as apheresis and bone marrow transplantation. With its unique characteristics in terms of being label-free, high-throughput, precise, and biocompatible, the 3D-AFT separation technology is well suited for a widely use of biological and biomedical applications, and potentially for clinical diagnostics as well as in point-of-care devices.

Supplementary Material

Refer to Web version on PubMed Central for supplementary material.

Acknowledgement

References

1. Whitesides G, Nature, 2006, 442, 368–373. [PubMed: 16871203]
2. Pamme N, Lab on a Chip, 2007, 7, 1644. [PubMed: 18030382]
3. Bhagat A, Bow H, Hou H, Tan S, Han J and Lim C, Medical & Biological Engineering & Computing, 2010, 48, 999–1014. [PubMed: 20414811]
4. Kwon K, Choi S, Lee S, Kim B, Lee S, Park M, Kim P, Hwang S and Suh K, Lab on a Chip, 2007, 7, 1461. [PubMed: 17960272]

5. Yamada M and Seki M, Lab on a Chip, 2005, 5, 1233. [PubMed: 16234946]

6. Sethu P, Sin A and Toner M, Lab Chip, 2006, 6, 83–89. [PubMed: 16372073]

7. Choi S, Song S, Choi C and Park J, Lab on a Chip, 2007, 7, 1532. [PubMed: 17960282]

8. Yamada M, Nakashima M and Seki M, Analytical Chemistry, 2004, 76, 5465–5471. [PubMed: 15362908]

9. Chen X, Cui D, Liu C and Li H, Sensors and Actuators B: Chemical, 2008, 130, 216–221.

10. Huang L, Science, 2004, 304, 987–990. [PubMed: 15143275]

11. Mach A and Di Carlo D, Biotechnology and Bioengineering, 2010, 107, 302–311. [PubMed: 20589838]

12. Lee M, Choi S and Park J, Journal of Chromatography A, 2011, 1218, 4138–4143. [PubMed: 21176909]

13. Hou H, Warkiani M, Khoo B, Li Z, Soo R, Tan D, Lim W, Han J, Bhagat A and Lim C, Scientific Reports, 2013, 3, 1259. [PubMed: 23405273]

14. MacDonald M, Spalding G and Dholakia K, Nature, 2003, 426, 421–424. [PubMed: 14647376]

15. Akagi T and Ichiki T, Analytical and Bioanalytical Chemistry, 2008, 391, 2433–2441. [PubMed: 18553186]

16. Gascoyne P and Vykoukal J, Electrophoresis, 2002, 23, 1973. [PubMed: 12210248]

17. Jubery T, Srivastava S and Dutta P, Electrophoresis, 2014, 35, 691–713. [PubMed: 24338825]

18. Hejazian M, Li W and Nguyen N, Lab on a Chip, 2015, 15, 959–970. [PubMed: 25537573]

19. Lenshof A, Magnusson C and Laurell T, Lab on a Chip, 2012, 12, 1210. [PubMed: 22362021]

20. Petersson F, Åberg L, Swärd-Nilsson A and Laurell T, Analytical Chemistry, 2007, 79, 5117–5123. [PubMed: 17569501]

21. Grenvall C, Magnusson C, Lilja H and Laurell T, Analytical Chemistry, 2015, 87, 5596–5604. [PubMed: 25909882]

22. Antfolk M, Antfolk C, Lilja H, Laurell T and Augustsson P, Lab on a Chip, 2015, 15, 2102–2109. [PubMed: 25824937]

23. Lin S, Mao X and Huang T, Lab on a Chip, 2012, 12, 2766. [PubMed: 22781941]

24. Shi J, Huang H, Stratton Z, Huang Y and Huang T, Lab on a Chip, 2009, 9, 3354. [PubMed: 19904400]

25. Ai Y, Sanders C and Marrone B, Analytical Chemistry, 2013, 85, 9126–9134. [PubMed: 23968497]

26. Ding X, Peng Z, Lin S, Geri M, Li S, Li P, Chen Y, Dao M, Suresh S and Huang T, Proceedings of the National Academy of Sciences, 2014, 111, 12992–12997.

27. Collins D, Alan T and Neild A, Lab Chip, 2014, 14, 1595–1603. [PubMed: 24638896]

28. Di Carlo D, Irimia D, Tompkins R and Toner M, Proceedings of the National Academy of Sciences, 2007, 104, 18892–18897.

29. Oakey J, Applegate R, Arellano E, Carlo D, Graves S and Toner M, Analytical Chemistry, 2010, 82, 3862–3867. [PubMed: 20373755]

30. Chung A, Gossett D and Di Carlo D, Small, 2012, 9, 685–690. [PubMed: 23143944]

31. Mao Z, Xie Y, Guo F, Ren L, Huang P, Chen Y, Rufo J, Costanzo F and Huang T, Lab on a Chip, 2016, 16, 515–524. [PubMed: 26698361]
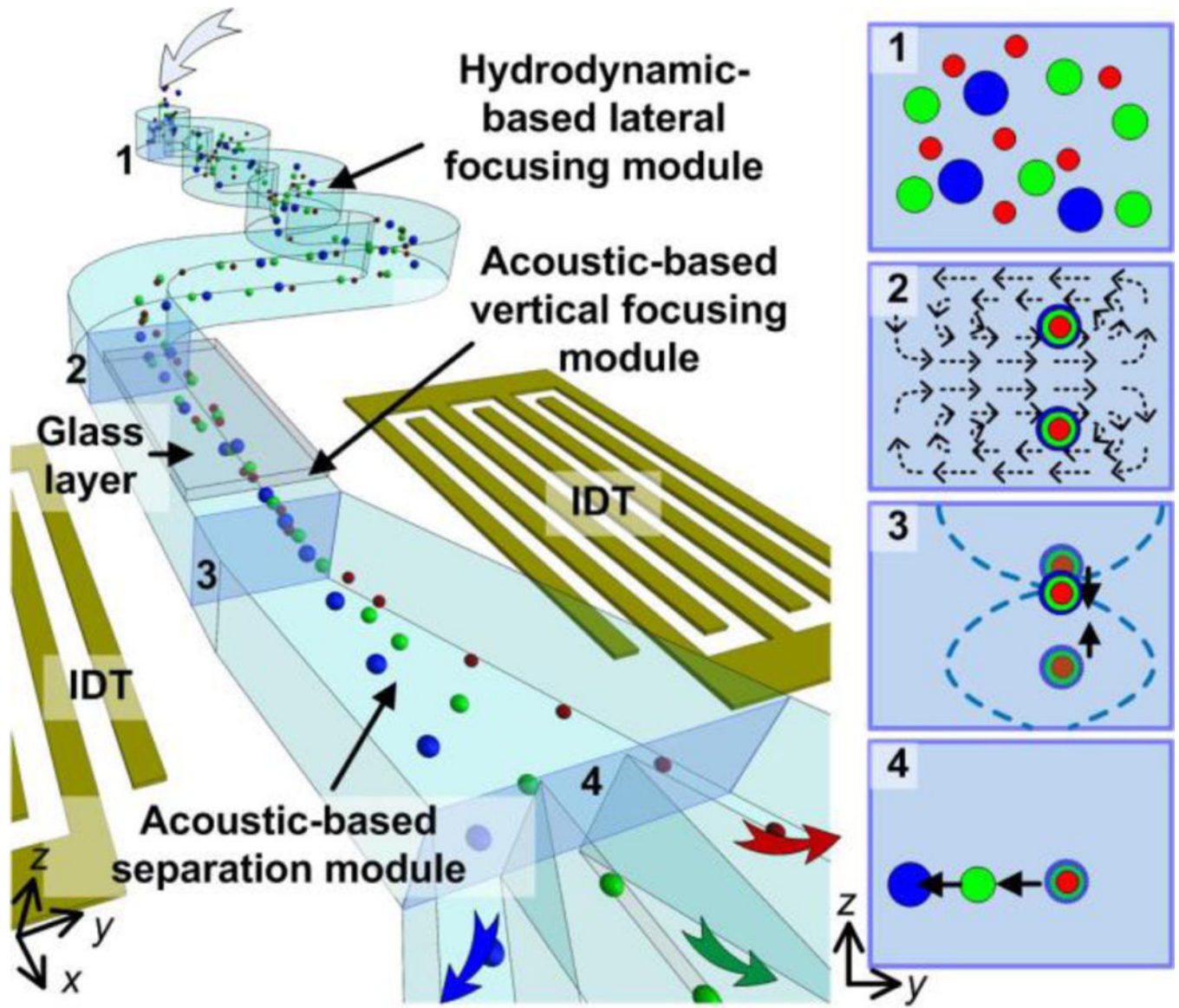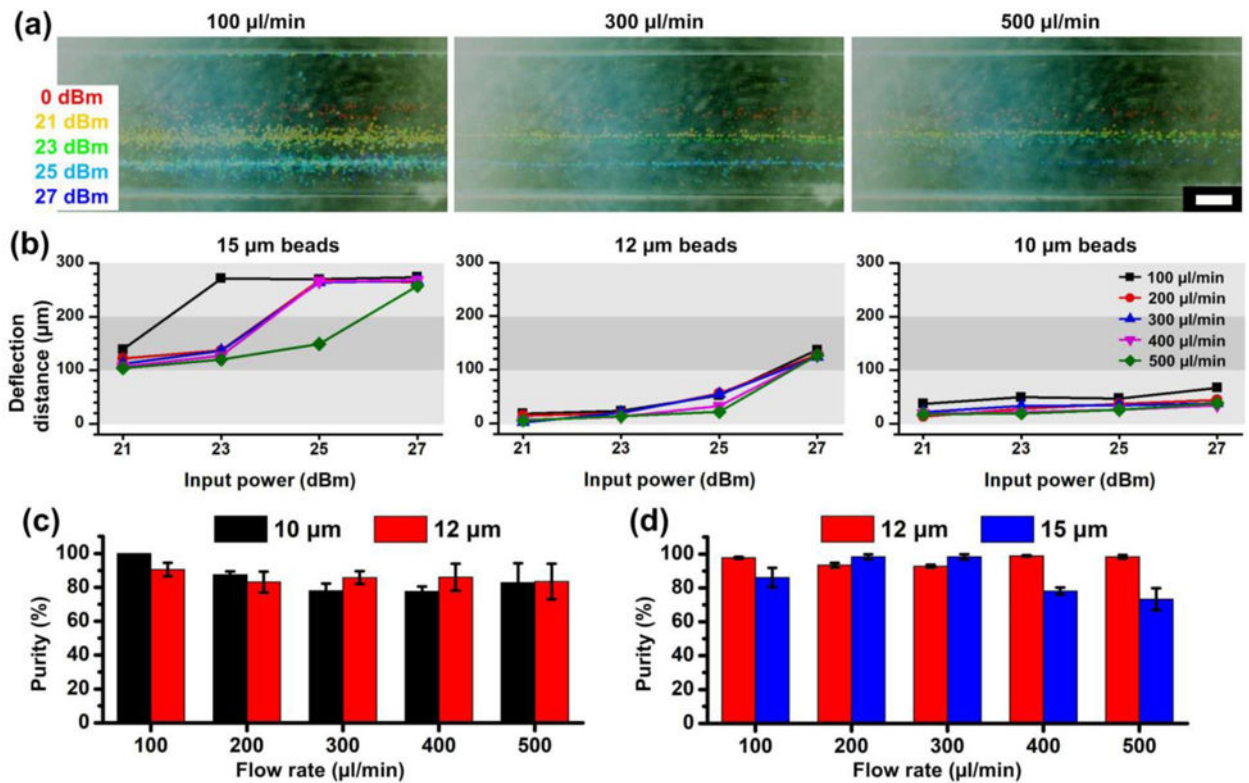
Figure 1.
Illustration of the 3D-AFT separation device. Particles are first ordered by a hydrodynamic focusing module, then aligned vertically by an acoustic focusing module. Finally, particles are sorted and separated to multiple outlets under the combined effects of acoustics and hydrodynamics.
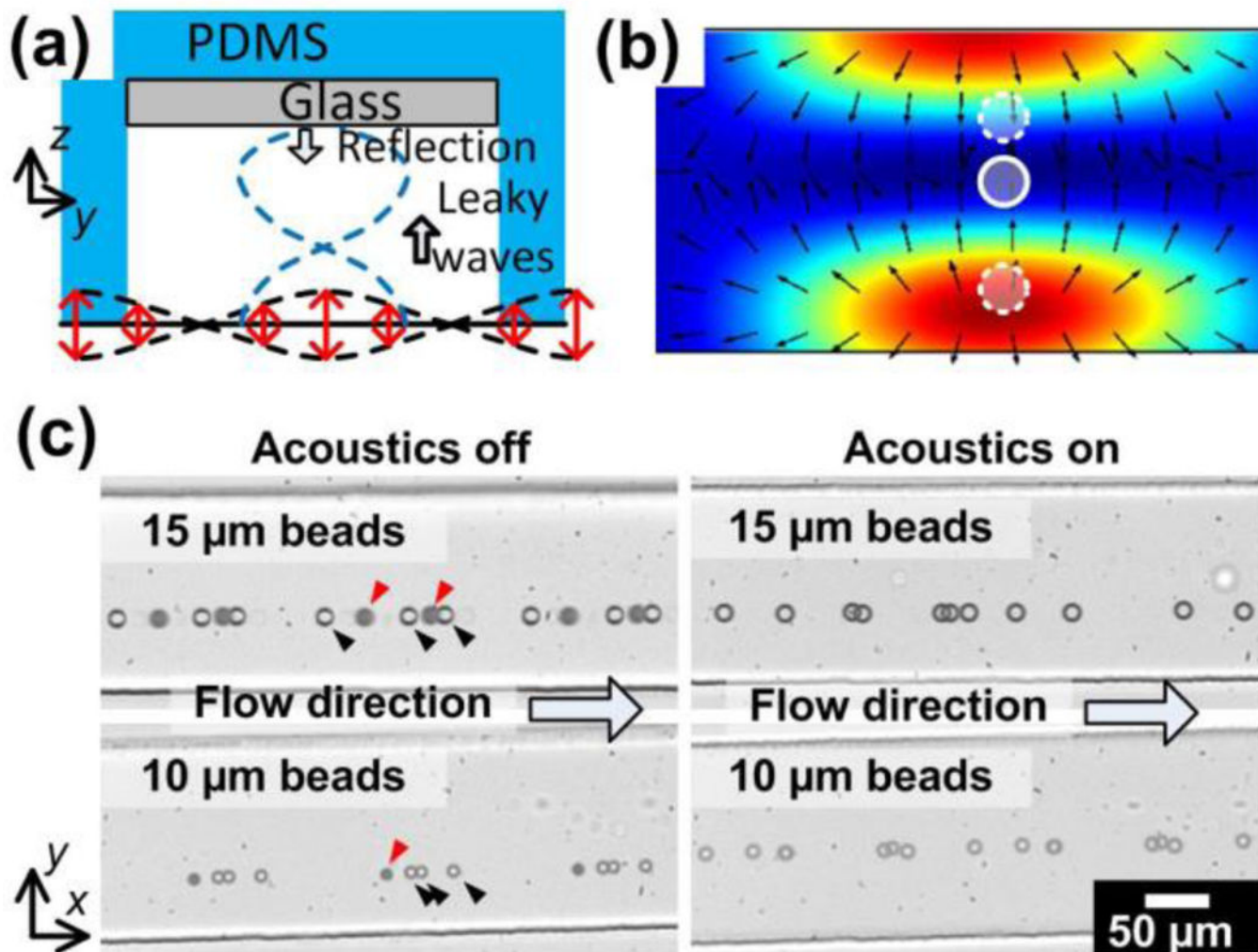
Figure 2.
Three-dimensional acoustic focusing of particles. (a) Illustration of the vertical acoustic resonator formed by the glass/PDMS hybrid channel. (b) Cross section showing the acoustic pressure distribution. (c) Stacked high-speed images of particles flowing through when the acoustic wave is off (left) and on (right).
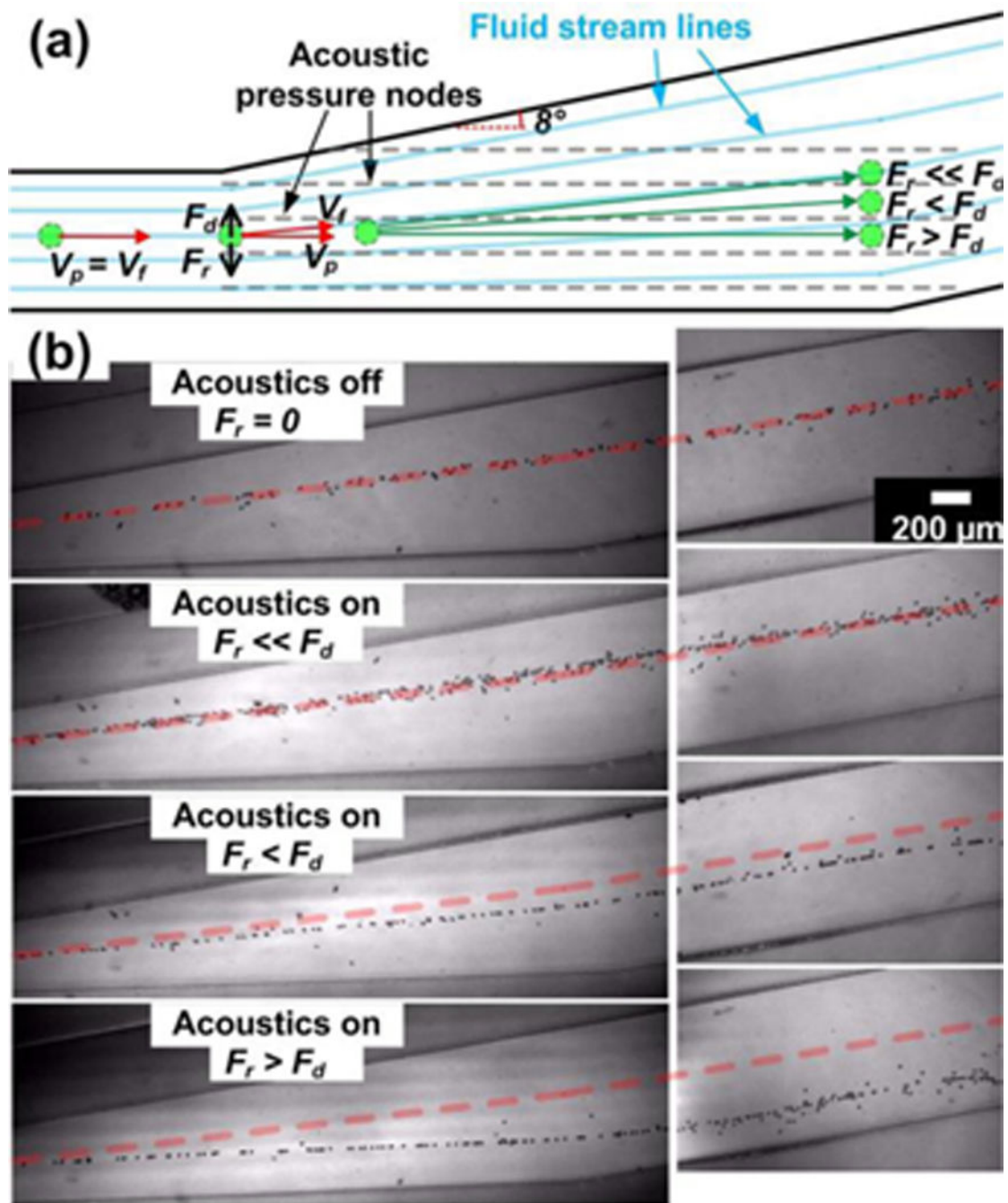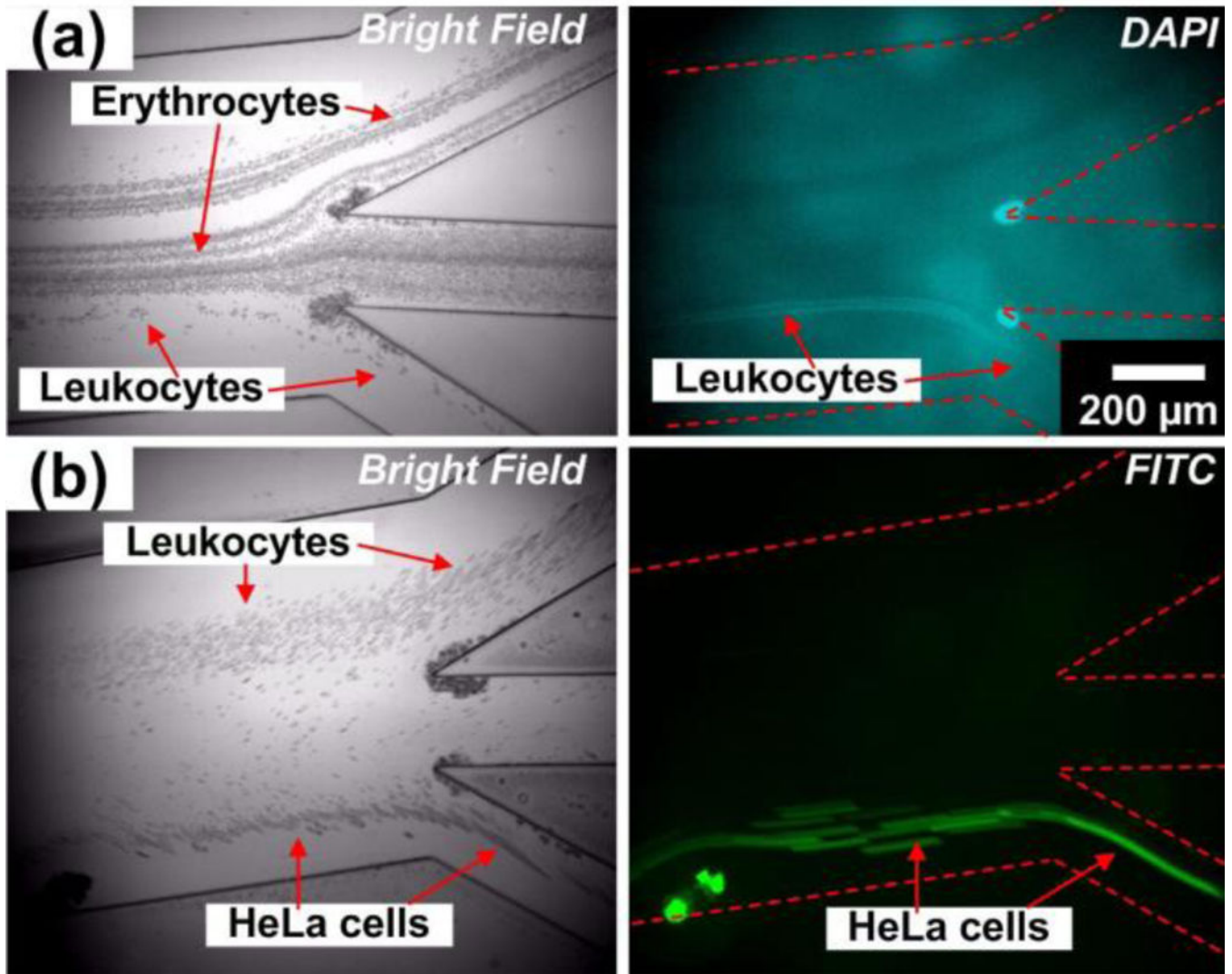
Figure 3.
Motions of particles are modulated precisely via 3D-AFT. (a) Schematic illustration of the 3D-AFT mechanism with respect to relative forces and velocities. (b) Experimental results of the modulation of particle motion by 3D-AFT. Each stacked image traces particle trajectories. The red dashed line is a reference indicating the particle trajectory when there is no acoustic excitation. The particle diameter is 15 μm.
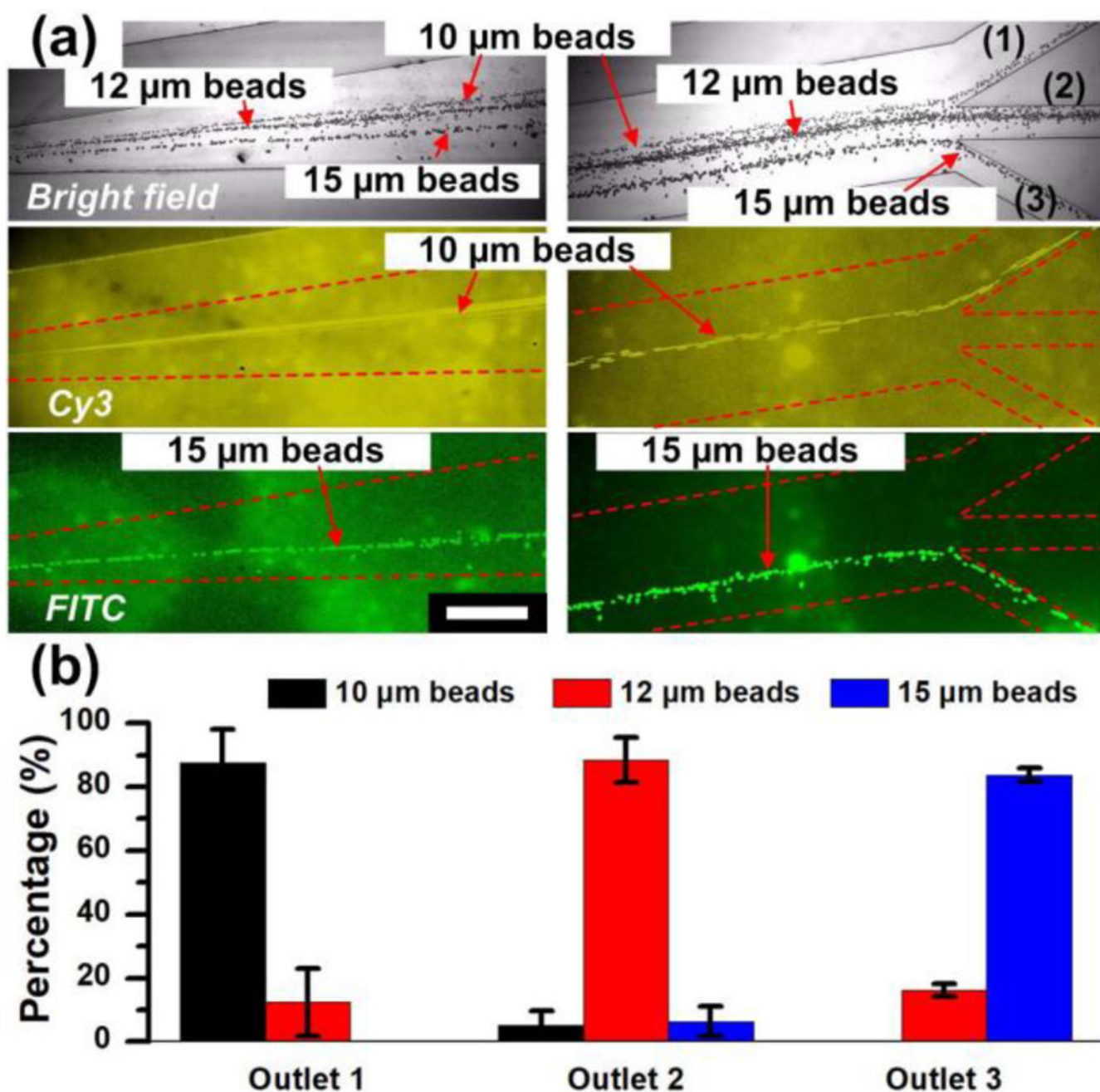
Figure 4.
The lateral shift in particle trajectories in the 3D-AFT device. (a) 15 μm particles migrate laterally via 3D-AFT separation device and the distance varies due to different input power amplitudes and flow rates. (b) Plots of the correlations between the deflection distance and the input power at various flow rates (n=1). Scale bar: 200 μm. (c) Separation performance of 10 μm / 12 μm particles and (d) 12 μm / 15 μm particles. The purity of outputs are characterized. The data is presented as average ± standard error (n=3).

Figure 5.
Acoustofluidic separation of cells via 3D-AFT. (a) Separation of erythrocytes and leukocytes which were tagged with DAPI for imaging purposes. (b) Isolating cancer cells (FITC conjugated) from leukocytes via 3D-AFT.

Figure 6.
Acoustofluidic separation of multiple fractions of different sized particles via 3D-AFT. (a) Stack images from video frame captures of bright field and two fluorescent fields show the trajectories of 10 μm (Cy3 conjugated), 12 μm and 15 μm (FITC conjugated) polystyrene beads. Scale bar: 500 μm. (b) Percentage of different sized beads collected from the three outlets. The data is presented as average ± standard error (n=3).